Measurement and Modeling of Electrode Biased Discharges in the HSX Stellarator

S.P. Gerhardt* 1), A.F. Almagri 1), D.T. Anderson 1), F.S.B. Anderson 1), D. Brower 2), J.M. Canik 1), C. Deng 1), W. Guttenfelder 1), K.M. Likin 1), V. Sakaguchi 1), J.N. Talmadge 1), K. Zhai 1)
1) HSX Plasma Laboratory, University of Wisconsin-Madison, USA
2) Electrical Engineering Department, University of California, Los Angeles, USA
e-mail contact of main author: sgerhard@pppl.gov

Abstract. Measurements of plasma flow damping have been conducted in the HSX stellarator. A fast-switching biased electrode system is used to impulsively generate plasma flow. Measurements of plasma flow using Mach probes and floating potential measurements with Langmuir probes are used to characterize the plasma response to the electrode. We observe two time-scales in the flow evolution, for both the bias turn-on and turn-off. The results are compared to neoclassical modelling, which also predicts two time-scales in the flow evolution. The spin-up rate is slower in the quasisymmetric configuration than in a configuration with the quasisymmetry broken, and is consistent with the neoclassical prediction for both configurations. The flows decay more slowly in the quasisymmetric configuration, but the decay rates are much larger than the neoclassical prediction. The measured radial conductivity also appears to be larger than the neoclassical prediction. These results indicate that although there appears to be some damping that cannot be explained by neoclassical theory, the damping of flows is reduced with quasisymmetry.

1. Introduction

The Helically Symmetric experiment (HSX) [1] is the first of a new generation of stellarators that exploit the concept of quasisymmetric magnetic fields. These configurations have a Fourier decomposition of |B| on a magnetic surface which is dominated by a single harmonic [2]. By introducing a direction of symmetry to the configuration, the neoclassical transport can be reduced to a level at or beneath a similar axisymmetric configuration. Among the many advantages of these configurations, there is minimal neoclassical damping of plasma flows in the direction of symmetry. This feature is in contrast to conventional stellarators, where the complicated variation in |B| in all directions on a magnetic surface may preclude large flows from developing.

Results in axisymmetric devices have indicated to importance of plasma flows for access to enhanced confinement regimes [3]. Plasma flow in the direction of symmetry in tokamaks (the toroidal flow) can be an important ingredient in the formation of both edge [3] and core [4] transport barriers. Hence, the reduction of flow damping in a stellarator may have a significant impact on the ability of these configurations to access enhanced confinement regimes. This route to improved confinement has been advocated in the design of the stellarators NCSX [4], CHS-qa [5], and QPS [6].

This paper presents the first evidence of a reduction in flow damping in a stellarator with quasisymmetry. Measurements of plasma flow damping rates have been made, and these results have been compared to neoclassical modelling. These results indicate that the flow damping is reduced in the quasisymmetric configuration compared to a configuration where the symmetry is broken, but that the flow damping is still larger than the neoclassical prediction.

* Present Affiliation: Princeton Plasma Physics Laboratory

The different magnetic field configurations of HSX [7] can be described by their Fourier decomposition (in Hamada coordinates [8]) on a magnetic surface

$$B = B_0 \sum_{n,m} b_{nm} \cos(m\alpha - n\zeta), \quad (1)$$

where α is the Hamada poloidal angle and ζ is the Hamada toroidal angle, and m and n are the poloidal and toroidal mode numbers respectively. In the quasihelically symmetric (QHS) [2] configuration, the spectrum is dominated by a single component with mode numbers (n,m)=(4,1). The quasisymmetry is broken in the Mirror configuration, where we introduce a second spectral component with mode numbers (n,m)=(4,0) and amplitude similar to the helical component. The viscous damping of plasma flows is expected to be significantly larger in the Mirror configuration compared to the QHS. The rotational transform, magnetic surface shapes, plasma volume, and magnetic well depth are all very similar between the two configurations [7].

In order to generate plasma flow in HSX, we use a biased electrode system [10]. The electrode generates a radial current flowing through the plasma, which causes a force on the plasma and thus plasma rotation. The electrode power supply is capable of applying voltage to the electrode in ~1μs at bias turn-on, and breaking the electrode current in ~1 μs at bias turn-off. We measure plasma flows with a system of multi-tipped Mach probes [10]. This system allows the simultaneous measurement of toroidal and poloidal flows with ~15μs time resolution. A seventh tip is built into the end of the probe, allowing local floating potential measurements to be made in addition to the flow measurements. For the measurements presented in this paper, the Mach probes were located in the region between the last closed magnetic surface (LCMS) and the surface on which the electrode resides; this is the region through which the radial current must flow.

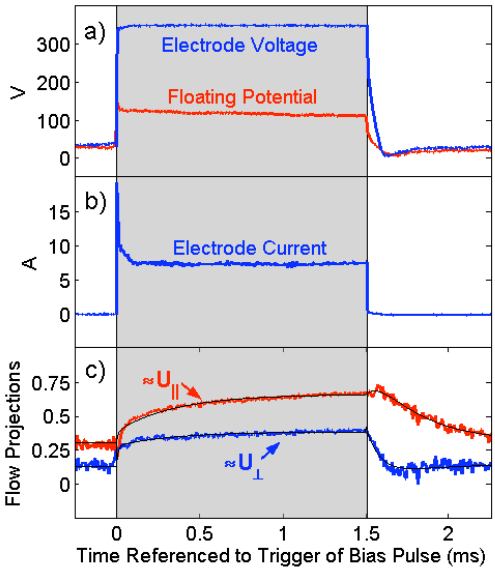

FIG. #1. The time evolution of a) the electrode voltage and floating potential, b) the electrode current, and c) the parallel and perpendicular flows, for the QHS case.

We use 28 GHz electron cyclotron heating at B=0.5 Tesla to form and heat plasma in HSX. The data presented in this paper is from plasmas with a line average plasma density of $1x10^{12}$ cm^{-3}, with hydrogen as the working gas. Typical plasma pulse lengths are 50 ms, allowing six independent bias pulses of 1.5 ms duration. The data shown in this paper are typically averages of 18-24 bias pulses from three or four repeatable discharges.

Two important quantities for the neoclassical theory can be measured spectroscopically: the neutral hydrogen density (to estimate the ion-neutral collision rate) and the ion temperature. The H_α emission from the plasma is determined using a set of 16 toroidally and poloidally distributed detectors [11]. The signal from these detectors is used to constrain the hydrogen source rate in the neutral gas code DEGAS [12], and we infer that the neutral hydrogen atom density is ~$1x10^{10}$ cm^{-3} in the discharges presented here. We measure an ion temperature of ~20eV from the Doppler broadened width of O^{+4} and O^{+1} spectral lines.

Given the tight collisional coupling between these impurity species and the majority protons, it is anticipated that their temperatures will be quite similar. This temperature is sufficient to place the ions in the plateau regime.

2. Details of the Plasma Flow Evolution

FIG. 1 illustrates the typical evolution during and after the bias pulse of the electrode voltage and current, the floating potential, and the plasma flows, for a QHS discharge. In this example the electrode is located at r/a~0.65 and the Mach probe is located at r/a~0.85. There are 18 identical bias pulses (6 pulses in each of three identical discharges) which are averaged to make this figure. When the electrode voltage is applied, the floating potential follows very quickly; we observe that the floating potential profile transitions to a new steady state within ~5 μs of the electrode voltage being applied. The electrode current shows a large transient before settling to its steady state value. The bottom frame of the figure illustrates the approximately parallel and perpendicular flows. There is a quick evolution of mainly the perpendicular flow, although there are smaller changes in the parallel flow on this fast rate as well; the rate for this fast evolution is faster than the Mach probe systems can measure. There is a second rate (~1-8 kHz) for the flow to evolve, mainly corresponding to evolution of the parallel flows.

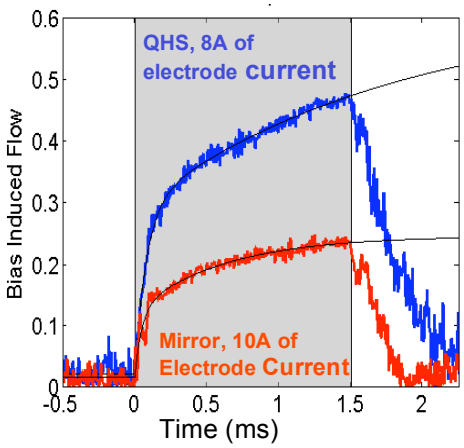

FIG. 2: Comparison of the flow evolution in the QHS and Mirror configurations. Flow speeds are in terms of the Mach number.

We open-circuit the electrode current to initiate the flow relaxation process; this is visible in the center frame of FIG. 1, where the electrode current is quickly terminated. The electrode becomes a large floating potential monitor once its current is terminated. Both the electrode voltage and floating potential at the Mach probe decay at a fast rate of ~30 kHz. The perpendicular component of the flow also decays at this fast rate, while the parallel part of the flow decays at a rate of ~3kHz. The asymmetry between the spin-up and relaxation phases is due to the different initiating events. For the spin-up, the electrode voltage application forces the electric field formation, and the plasma flows and electrode current respond. The electrode current is terminated to start the relaxation phase, and the electric field and flows respond. In each case there are two time-scales for the flows to evolve, with the perpendicular flows generally following the floating potential evolution.

In order to extract time-scale information from this data, a two direction/two time-scale fit technique has been developed. It is assumed that the flow rises in a direction **f** at a fast rate (r_f) and in a direction **s** at a slower rate (r_s):

$$\mathbf{U}(t) = C_f\left(1-\exp\left(-r_f t\right)\right)\mathbf{f} + C_s\left(1-\exp\left(-r_s t\right)\right)\mathbf{s}. \qquad (2)$$

The directions (**f** and **s**), flow magnitudes (C_f and C_s), and rates (r_f and r_s) are free parameters when fitting (2) to the flow measurements. A second step is used to fit the decay with the modification in (2): $1-\exp(-rt) \rightarrow \exp(-r(t-t_o))$, with t_o the time when the electrode current is terminated. The spin-up and decay fits obtained using this method are illustrated as thin lines in the bottom frame of FIG. 1.

We have studied the flow evolution in QHS and Mirror discharges where all properties (line average density, ion temperature, magnetic field strength on axis, and ECH power) are similar except the magnetic geometry. An example of the flow evolution (in Mach number) in the two configurations is shown in FIG. 2, where 340 V of bias was applied at r/a≈0.7. After a similar initial rise, the flow in the QHS configuration takes longer to rise, but goes to a larger value. Given that ≈8A of current was drawn in the QHS case and ≈10A in the Mirror case, the quasisymmetric configuration exhibits more flow per unit torque. When the electrode current is terminated, the flow in the QHS case decays more slowly than in the Mirror. All of these features are indicative of reduced flow damping in the quasisymmetric configuration.

3. Neoclassical Modeling of the Plasma Flow Evolution

The model used in this research is motivated by the work of Coronado and Talmadge [13]. This model describes the damping of plasma flows in a non-axisymmetric torus, including the effect of ion-neutral friction. The calculation begins with the parallel and poloidal momentum balance equations,

$$m_i N_i \frac{\partial}{\partial t} < \mathbf{B}\cdot\mathbf{U} > = - < \mathbf{B}\cdot\nabla\cdot\Pi > - m_i N_i \upsilon_{in} < \mathbf{B}\cdot\mathbf{U} >, \tag{3}$$

$$m_i N_i \frac{\partial}{\partial t} < \mathbf{B}_P\cdot\mathbf{U} > = -\frac{\sqrt{g}B^\xi B^\alpha}{c} < \mathbf{J}_{plasma}\cdot\nabla\psi > - < \mathbf{B}_P\cdot\nabla\cdot\Pi > - m_i N_i \upsilon_{in} < \mathbf{B}_P\cdot\mathbf{U} >, \tag{4}$$

on each flux surface independently. In these expressions, m_i is the ion mass, N_i is the ion density, U is the flow speed, ν_{in} is the ion neutral collision frequency, $\mathbf{B}_P = B^\alpha \mathbf{e}_\alpha$ is the Hamada poloidal magnetic field, B^α and B^ξ are the contravariant poloidal and toroidal magnetic fields, $\mathbf{e}_\alpha$ is the covariant poloidal basis vector, ψ is the toroidal flux, $\sqrt{g}$ is the Jacobian, and c is the speed of light. The currents flowing through the plasma and the electrode ($\mathbf{J}_{plasma}$ and $\mathbf{J}_{ext}$, respectively) are related to the electric field through Ampere's law.

$$\frac{\partial}{\partial t}\frac{\partial \Phi}{\partial \psi} < \nabla\psi\cdot\nabla\psi > = 4\pi\left(< \mathbf{J}_{plasma}\cdot\nabla\psi > + < \mathbf{J}_{ext}\cdot\nabla\psi > \right). \tag{5}$$

The neoclassical viscosities in (3) and (4) can be written in the plateau regime [14,15] as $<\mathbf{B}\cdot\nabla\cdot\boldsymbol{\Pi}> = \mu_\alpha B^\alpha + \mu_\xi B^\xi$ and $<\mathbf{B}_P\cdot\nabla\cdot\boldsymbol{\Pi}> = \mu_\alpha^{(P)} B^\alpha + \mu_\xi^{(P)} B^\xi$, where $\mu_\alpha = \kappa(B^\alpha \alpha_P + B^\xi \alpha_C)$, $\mu_\xi = \kappa(B^\alpha \alpha_C + B^\xi \alpha_T)$, $\mu_\alpha^{(P)} = \kappa B^\alpha \alpha_P$, and $\mu_\xi^{(P)} = \kappa B^\alpha \alpha_C$ Terms in the viscosities proportional to the heat flows are neglected in this model. The viscosity coefficients use $\kappa = \pi^{1/2} P B_o / \nu_t B^\xi$, $\alpha_T = \Sigma n^2 b_{n,m}^2 / |n - m\iota|$, $\alpha_p = \Sigma m^2 b_{n,m}^2 / |n - m\iota|$, and $\alpha_C = -\Sigma nm b_{n,m}^2 / |n - m\iota|$, where P is the pressure, ν_t is the thermal velocity, and the sums are over all spectral components except the (n,m)=(0,0) component. These viscosities are strictly correct for time scales longer than the ion-ion collision time [16], implying that the modelled time scales are only correct for times $\tau > 0.1$ms (for HSX parameters).

In steady state, this modeling predicts the relationship between $\mathbf{J}_{plasma}$ (=$\mathbf{J}_{electrode}$) and the electric field as

$$\left\langle \mathbf{J}_{plasma}\cdot\nabla\psi \right\rangle = \sigma_\perp \left(\left\langle \mathbf{E}_r\cdot\nabla\psi \right\rangle - \frac{\left\langle \nabla p_i\cdot\nabla\psi \right\rangle}{eN_i} \right), \tag{6}$$

where the radial conductivity is calculated as

$$\sigma_{\perp} = \frac{c^2 m_i N_i \left\langle B_P^2 \right\rangle}{\left\langle \nabla\psi \cdot \nabla\psi \right\rangle \left(\sqrt{g} B^{\alpha} B^{\zeta} \right)^2 \left(\text{ł}\upsilon_{\alpha} + \upsilon_{\zeta} + \upsilon_{in} \frac{\left\langle B^2 \right\rangle}{\left\langle B^2 \right\rangle} \right)} \left[\begin{array}{l} \left(\upsilon_{\alpha}^{(P)} + \upsilon_{in} \frac{\left\langle \mathbf{B}_P \cdot \mathbf{B}_P \right\rangle}{\left\langle B_P^2 \right\rangle} \right) \left(\upsilon_{\zeta} + \upsilon_{in} \frac{\left\langle \mathbf{B} \cdot \mathbf{B}_T \right\rangle}{\left\langle B^2 \right\rangle} \right) - \\ \left(\upsilon_{\zeta}^{(P)} + \text{ł}\upsilon_{in} \frac{\left\langle \mathbf{B}_P \cdot \mathbf{B}_T \right\rangle}{\left\langle B_P^2 \right\rangle} \right) \left(\upsilon_{\alpha} + \upsilon_{in} \frac{\left\langle \mathbf{B} \cdot \mathbf{B}_P \right\rangle}{\text{ł}\left\langle B^2 \right\rangle} \right) \end{array} \right] . \quad (7)$$

We have developed a new model to explain the spin-up process [7], based on the observation in FIG. 1. In this model, the spin-up is initiated by a quick rise of the electric field. Radial force balance indicates that **E**x**B** flows will grow on the time-scale that the electric field is applied. Incompressibility of the ion fluid causes compensating Pfirsch-Schlueter like flows to grow on the same time-scale. The parallel momentum balance shows that a second component of the flow grows in the parallel direction on a "hybrid" rate υ_F:

$$\upsilon_F = \text{ł}\upsilon_{\alpha} + \upsilon_{\zeta} + \upsilon_{in} \quad (8)$$

The viscous frequencies in this expression are defined as a poloidal viscous damping frequency $\nu_{\alpha}=\mu_{\alpha}B^{\zeta}/m_iN_i\langle \mathbf{B}\cdot\mathbf{B}\rangle$ and a toroidal viscous damping frequency $\nu_{\alpha}=\mu_{\zeta}B^{\zeta}/m_iN_i\langle \mathbf{B}\cdot\mathbf{B}\rangle$. We see that this damping rate ν_F is determined by damping in both the toroidal and poloidal directions, and can anticipate that it will be faster than the damping of flows in the direction of symmetry. The poloidal momentum balance equation is the final constraint in the model, and predicts that a transient will occur in the electrode current before it settles to a steady state value, in a fashion similar to that in FIG. 1.

We follow the formulation of Coronado and Talmadge [13] in modeling the decay of the plasma flows and electric field when the electrode current is terminated. The model predicts that there will be two rates for the plasma flows and electric field to decay, given by

$$\left. \begin{matrix} \gamma_s \\ \gamma_f \end{matrix} \right\} = -\upsilon_{in} - \frac{\upsilon_1 - I_o \upsilon_{in}}{2\Omega} \pm \left[\left(\frac{\upsilon_1 - I_o \upsilon_{in}}{2\Omega} \right)^2 + \frac{\upsilon_{in} I_o \left(\text{ł}\upsilon_{\alpha} + \upsilon_{\zeta} \right) + \upsilon_{\zeta}^{(P)} \upsilon_{\alpha} - \upsilon_{\alpha}^{(P)} \upsilon_{\zeta}}{\Omega} \right]^{1/2} , \quad (9)$$

where $I_o = \left(B^{\alpha} / 2\pi \right)^2 \left\langle \nabla\rho \cdot \nabla\rho \right\rangle / \left(4\pi m_i N_i \left\langle \mathbf{B}_p \cdot \mathbf{B}_p \right\rangle \right)$ and $\Omega = 1 + I_o - \left\langle \mathbf{B} \cdot \mathbf{B}_p \right\rangle^2 / \left(\left\langle \mathbf{B}_p \cdot \mathbf{B}_p \right\rangle \left\langle \mathbf{B} \cdot \mathbf{B} \right\rangle \right)$. The viscous frequencies are defined as $\upsilon_{\alpha}^{(P)} = \mu_{\alpha}^{(P)} B^{\alpha} / m_i N_i \left\langle \mathbf{B}_p \cdot \mathbf{B}_p \right\rangle$ and $\upsilon_{\zeta}^{(P)} = \mu_{\zeta}^{(P)} B^{\alpha} / m_i N_i \left\langle \mathbf{B}_p \cdot \mathbf{B}_p \right\rangle$, and the frequency ν_1 is given by

$$\upsilon_1 = \upsilon_{\alpha}^{(P)} + (1 + I_o) \left(\text{ł}\upsilon_{\alpha} + \upsilon_{\zeta} \right) - \frac{\left\langle \mathbf{B} \cdot \mathbf{B}_P \right\rangle}{\left\langle \mathbf{B} \cdot \mathbf{B} \right\rangle} \left(\upsilon_{\alpha}^{(P)} + q\upsilon_{\zeta}^{(P)} \right) - \frac{\left\langle \mathbf{B} \cdot \mathbf{B}_P \right\rangle}{\left\langle \mathbf{B}_P \cdot \mathbf{B}_P \right\rangle} \text{ł}\upsilon_{\alpha} . \quad (10)$$

It can be shown that the slower rate (γ_s) corresponds to the damping of plasma flow in the direction of symmetry [7]; this rate goes to zero in the limit of perfect quasisymmetry with no neutrals. The faster rate (γ_f) corresponds to damping of flows across the contours of constant |B| and their accompanying parallel flows [7].

FIG. 3 shows the three neoclassical rates, for both the QHS and Mirror configurations. The calculations were made with plasma parameters similar to those in the experiment, except that the ion-neutral collision frequency has been set to zero to emphasize the difference in parallel viscous damping between these configurations. The neoclassical slow decay rate shows the largest difference between the QHS and Mirror configurations. The ratio of the slow rates for the two configurations is ~100, reducing to ~10 at the LCMS. The hybrid rate ν_F lies between the fast and slow rates for both configurations. Note that the difference in ν_F

between the QHS and Mirror configurations goes from a factor of ~100 in the core to only ~40% at the LCMS.

The modelling discussed above requires the calculation of terms like $\langle \mathbf{B}\cdot\mathbf{B}\rangle$, $\langle \mathbf{B_P}\cdot\mathbf{B_T}\rangle$, and $\langle \mathbf{B_P}\cdot\mathbf{B_P}\rangle$. Previous applications of neoclassical modelling have often used the basis vectors of a large aspect ratio tokamak [17] as an approximation to the stellarator basis vectors. While this may be a reasonable approximation for a conventional stellarator with a toroidal curvature component in the magnetic field spectrum, HSX was expressly designed to eliminate this field modulation. We have developed a method to calculate the Hamada basis vectors for arbitrary toroidal geometry [7] and applied the method to the QHS and Mirror configurations of HSX. This technique allows the accurate calculation of the aforementioned flux surface averages, as well as enabling detailed comparisons between measured and predicted flow directions [7].

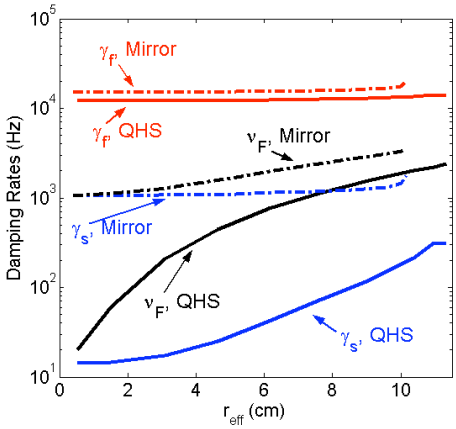

FIG.3. Comparison of the calculated neoclassical damping rates for the QHS and Mirror configurations.

4. Comparison Between the Measurements and Modeling

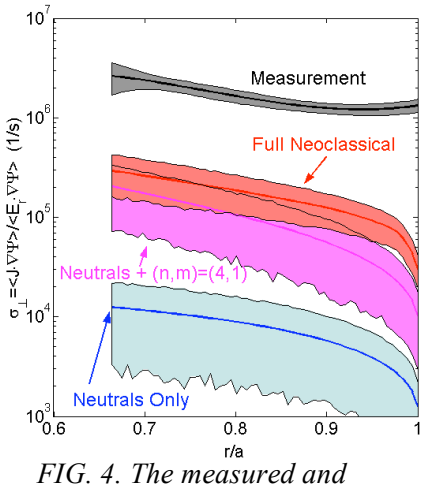

FIG. 4. The measured and predicted radial conductivity profiles in the QHS configuration with line average density of $1x10^{12}$ cm^{-3}.

FIG. 4 illustrates the comparison between the measured and modeled radial conductivity for the QHS configuration. To measure the radial conductivity, we use (6), where the electric field is inferred from the floating potential gradient, the ion pressure gradient is neglected, and it is assumed that $\langle J_{plasma}\cdot\nabla\psi\rangle = I\langle\nabla\psi\rangle/A_{surf}$, where A_{surf} is the area of a flux surface. There are three neoclassical predictions shown in the figure. The bottom curve is the radial conductivity calculated using equation (7) with neutrals only; all of the viscous frequencies are set to zero. The next higher curve shows the radial conductivity considering both neutrals and the main helical spectral component. The combination of neutral friction and a single magnetic field modulation causes a significant increase in radial conductivity in the plateau regime [18]. The uppermost neoclassical prediction shows the radial conductivity including neutrals and the complete magnetic field spectrum. The ratio of the measured to the total prediction is a factor of 10; we thus infer that the radial conductivity is anomalous. Note that the uncertainty bands in this and subsequent calculations are based on Monte Carlo propagation of the estimated uncertainty in input parameters such as the ion temperature, plasma density, and neutral density.

Rozhansky and Tendler [19] have derived an expression for the radial conductivity in a circular cross section tokamak, where the toroidal flows are damped by anomalous shear viscosity. Their model agrees reasonable well with the radial conductivity in L-mode in the TUMAN-3 tokamak [20], and we have found that their prediction generally agrees with the HSX measurements to within a factor of two. The extension of their model to the stellarator geometry is a subject for further research.

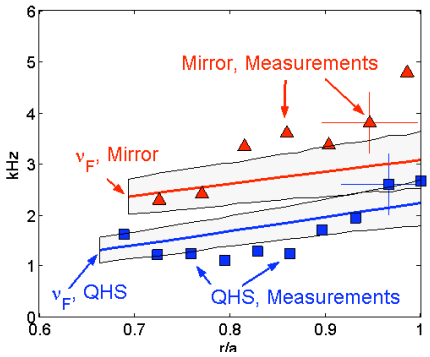

FIG. 5: Measured slow flow spin-up rates in the QHS and Mirror configurations and the theoretical rate given by

We have made detailed profiles of the flow evolution in the QHS and Mirror configurations, and used the fitting of equation (2) to extract the time-scales from the data. The radial profile of the slow rate for the flows to rise (r_s from the flow rise fits of (2)), is shown in FIG. 5 for the QHS and Mirror configurations. The flow rises more slowly in the QHS configuration at all points across the minor radius, indicating a reduction in damping. The hybrid rate ν_F is shown for the two cases as well, illustrating the excellent agreement between the modeling and measurement. The difference in ν_F between the two calculations is due to the difference in neoclassical parallel viscosity, implying that the difference in the measurements is a neoclassical effect as well.

It was observed near FIG. 1 that the floating potential and the fast component of the flow decay on a time-scale of 30-50μs. In contrast with the neoclassical prediction, we do not observe a slower decay in the floating potential or electric field. Furthermore, the neoclassical prediction is that the slowly decaying component of the flow should be in the symmetry direction, while we observe that the slowly decaying component of the flow is mainly in the parallel direction. FIG. 6 illustrates a profile of the slower decay rate (r_s from the decay fits) for the QHS and Mirror configurations. The flows take longer to decay in the QHS configuration, as expected for a configuration with reduced damping. The *difference* in damping rates is ~2-3x10^3 s^{-1}.

The figure also shows the slow neoclassical damping rate (γ_s). In the QHS configuration, this rate is dominated by ion-neutral collisions, and is ~250 s^{-1}. The flows decay more quickly than the neoclassical prediction by a factor of ~10. The slow damping rate in the Mirror configuration also differs from the neoclassical prediction, although the ratio of measurement to prediction is a factor of ~5 in this case. The *difference* in the neoclassical prediction of ~1.5x10^3 s^{-1} is similar to the *difference* in the measurements. We infer from this observation that there may be some source of extra flow damping which obscures most, but not all, of the predicted neoclassical difference between the configurations. This result is in keeping with the results from axisymmetric systems, where it has been demonstrated in large [21,22] and medium [20] size tokamaks that the damping of plasma flows in the toroidal direction is anomalously fast.

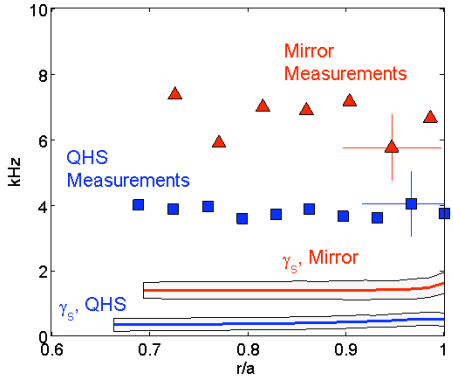

FIG. 6: Measured slow flow decay rates in QHS and Mirror configurations and comparison to the prediction of Equation 7.

We have constructed two Mach probes, to make simultaneous flow measurements in the high and low |B| regions of the machine (both of which are accessible from the outboard side, due to the helical symmetry. We have found the rates for the flows and floating potential evolution to be the same in both regions. We thus conclude that these time-scales are global quantities, as predicted in the modeling.

5. Summary

Our results indicate an asymmetry between the spin-up and relaxation phases of the biased electrode experiment. The application of the electrode bias causes an electric field to form and a transient is observed in the electrode current; the fast open-circuiting of the electrode current allows a slower decay (~30-50μs) of the electric field. In each case, two time-scales are observed in the evolution of the plasma flow, and a technique has been developed to extract the time-scale information for the measured flow evolution. The flows in the QHS configuration are observed to evolve more slowly than those in the Mirror configuration, and to have more flow per unit torque than in the Mirror configuration. These observations are consistent with there being reduced damping of flows in the quasisymmetric case. The spin-up rates are consistent with a neoclassical model where a quick change in the electric field initiates the spin-up process. The rate at which the flow decays is faster and the radial conductivity is larger than the neoclassical prediction.

The authors gratefully acknowledge the advice and assistance of C. Hegna, K.C. Shaing, A. Piccione, M. Frankowski, E. Jolitz and P. Probert. This research was funded by the United States Department of Energy.

References:

[1] ANDERSON, F.S.B., et al., Fusion Technology **27**, (1995) 273.
[2] NUHRENBERG, J. and ZILLE, R., Physics Letters A **129**, (1988) 113.
[3] BURRELL, K.H., Phys. Plasmas **4**, (1997) 1499.
[4] SYNAKOWSKI, E. J., et al., Nuclear Fusion **39**, (1995) 1733.
[5] ZARNSTORFF, et al., Plasma Phys. Control. Fusion **43**, (2001) 237.
[5] OKAMURA, S., et al., Nuclear Fusion **41**, (2001) 1865.
[6] SPONG, D.A., Nuclear Fusion **41**, (2001) 711.
[7] GERHARDT, S.P., Measurements and Modelling of Plasma response to Electrode biasing in the HSX Stellarator, PhD Thesis, Univ. of Wisconsin, Madison (2004).
[8] D'HAESELEER, W.D., et al., Flux Coordinates and Magnetic Field Structure, Springer-Verlag, Berlin (1991).
[10] GERHARDT, S.P., et al, Electrode and Langmuir Probe Tools used for Flow Damping Studies in HSX, Rev. Sci. Instrum. (in press).
[11] GERHARDT, S.P., et al, Rev. Sci. Intrum. **75**, (2004) 2981
[12] HEIFETZ, D.B., et al. J. Comp. Phys. **46,** (1982) 309.
[13] CORONADO, M., and TALMADGE, J.N., Phys. Fluids B **5**, (1993) 1200.
[14] SHAING, K.C., HIRSHMAN, S.P., and CALLEN, J.D., Phys. Fluids **29**, (1986) 521.
[15] CORONADO, M and WOBIG, H., Phys. Fluids **29**, (1986) 527.
[16] HIRSHMAN, S.P., Nuclear Fusion **18**, (1978) 917.
[17] CORONADO, M. and TREJO, J.G., Phys. Fluids B **2**, (1990) 530.
[18] TALMADGE, J.N., et al., Proceedings of the 15th International Conference on Plasma Physics and Controlled Fusion Research (Seville, 1994), IAEA, Vienna, **1** (1995) 797.
[19] V. ROZHANSKY, and M. TENDLER, Phys. Fluids B **4**, (1992) 1877.
[20] ASKINAZI, L.G., et al., Nuclear Fusion **32**, (1992) 271.
[21] SCOTT, S.D. et al., Phys. Rev. Lett. **64**, (1990) 531.
[22] DEGRASSIE, J.S. et al., Nuclear Fusion **43**, (2003) 142.